IMPLEMENTING REGENERATIVE ENERGY RECOVERY IN ELECTRIC VEHICLES USING DYNAMIC LOGIC THRESHOLD CONTROL

Rong SU[1], Zongjun YIN[2,*], Ru WANG[3,*], Xuegang MA[4]

Regenerative braking technology held immense potential for reducing energy consumption in electric vehicles. This paper focused on enhancing the efficiency of regenerative braking systems in electric vehicles equipped with integrated front-wheel drive configurations. Firstly, the allocation of braking force between the front and rear axles was determined through integrating the I-curve characteristics of an electric vehicle with the European Economic Commission (ECE) regulations, with the goal of ensuring optimal braking stability. Secondly, the peak regenerative braking torque produced by the motor was established through an analysis of the motor's torque capabilities and the charging capacity of the battery. A comprehensive assessment was conducted to determine the distribution of regenerative and hydraulic braking torques that contribute to the total braking torque on the front axle, utilizing a logic strategy. The logic threshold was continuously updated based on real-time factors such as braking intensity, battery state of charge, and vehicle speed. This ensured that the regenerative braking system operated within its optimal range while maintaining safe and efficient braking performance. To validate the proposed control strategy, a regenerative braking model was developed by incorporating the aforementioned braking force distribution scheme. The model was tested under two standard driving cycles: World Light-Duty Vehicle Test Cycle (WLTC) and China Light-Duty Vehicle Test Cycle-Passenger (CLTC-P). The results demonstrated significant improvements in regenerative braking efficiency across all driving conditions. Remarkably, the regenerative braking efficiency consistently exceeded 40% in two cycles. Our study holds considerable significance in the quest to enhance energy efficiency and boost the driving range of electric vehicles, thereby mitigating the environmental impact of transportation and promoting a sustainable future.

Keywords: regenerative braking, dynamic logic threshold, real-time factors, energy recovery, driving cycles

[1] School of Mechanical Engineering, Anhui Institute of Information Technology, Wuhu 241100, China, 2019006788@aiit.edu.cn
[2] School of Mechanical Engineering, Anhui Institute of Information Technology, Wuhu 241100, China, yinzongjunyzj@163.com
[3] School of Mechanical Engineering, Anhui Institute of Information Technology, Wuhu 241100, China, 2023002600@aiit.edu.cn
[4] School of Mechanical Engineering, Anhui Institute of Information Technology, Wuhu 241100, China, 2015055@aiit.edu.cn
*Corresponding authors: Zongjun YIN and Ru WANG

1. Introduction

Regenerative braking of vehicles refers to the process of converting kinetic energy into electrical energy through an electric motor during braking [1]. This technology can improve vehicle energy efficiency and reduce energy waste and environmental pollution [2]. Regenerative braking in electric vehicles is a complex system affected by several key components and factors [3]. Firstly, the electric motor's braking capability, power generation capacity, and efficiency directly influence the amount of energy recovered [4]. Secondly, the energy storage device, such as batteries, capacitors, or flywheels, is essential for storing the regenerated energy [5]. Moreover, the control strategy dictates the amount of energy that can be recovered through regenerative braking [6]. Lastly, the operating environment, including road conditions and vehicle status, significantly influences the performance of regenerative braking [7].

In electric vehicles, the energy recovery system adeptly integrates regenerative braking with hydraulic braking. However, it encounters two significant challenges [8]. The first challenge is achieving the optimal balance between regenerative braking and mechanical braking [9]. This entails determining the ideal distribution of braking force between the two systems to maximize energy recovery while ensuring safe and stable braking performance. The objective is to maximize the use of regenerative braking without compromising the vehicle's capacity to decelerate effectively under all driving conditions. Secondly, maintaining stable braking necessitates the proper distribution of braking forces between the front and rear axles [10]. This balance is crucial to ensure smooth and predictable braking, thereby preventing any negative effects such as skidding or instability. By effectively tackling these two challenges, electric vehicles can significantly enhance their energy efficiency during dynamic driving scenarios [11].

There are many control algorithms for regenerative braking, such as PID, optimal, neural network, fuzzy controls, etc. The control algorithms can be chosen and utilized based on the particular needs and effectiveness of the regenerative braking system [12]. Dynamic logic threshold approach offers significant advantages in regenerative braking systems compared to classical fixed threshold method [13]. By adapting to changing driving conditions, such as vehicle speed, vehicle states, and road conditions, optimizing braking performance. This real-time adjustment maximizes energy recovery by selecting the optimal regenerative braking intensity, preventing over-braking or under-braking [14].

This paper presents a novel regenerative braking control strategy designed specifically for front-wheel-drive pure electric vehicles. The main objective of this strategy is to enhance energy utilization efficiency and minimize the environmental footprint of electric vehicles. The proposed control strategy relies on a dynamic

logical threshold control method to effectively allocate braking forces between the motor and hydraulic systems of the front axle. By establishing a maximum threshold for the braking torque of the front axle motor, the strategy ensures stable and efficient regenerative braking performance. Furthermore, the control strategy optimizes the participation of the regenerative braking, taking into account factors such as brake strength, battery state of charge, and vehicle speed. This optimization process aims to maximize energy recovery during braking, thereby improving the overall energy efficiency of the vehicle.

2. Electric vehicles equipped with a regenerative braking mechanism

2.1. Development of motorized hydraulic brake system

Vehicles can be categorized into three types based on their driving configurations: front-wheel drive (FWD), rear-wheel drive (RWD), and four-wheel drive (4WD). These different driving methods exhibit distinct advantages and disadvantages. Among them, front-wheel drive electric vehicles have a substantial market share, primarily because they utilize front-wheel drive to deliver power, positioning the electronic control system and electric drive system at the front of the vehicle. This configuration not only saves space but also reduces the need for a driveshaft, which can lower costs to some extent. Electric vehicles frequently use a front-wheel drive power-train system, providing a small installation size and improved transmission efficiency [15]. The brake system consists of two main parts: a traditional hydraulic brake system and a regenerative brake system. As depicted in Fig. 1, the control system architecture is organized into two hierarchical layers, each with distinct responsibilities.

The brake controller assembly is a critical component within the first layer of the system, as it is responsible for distinguishing between two key braking methodologies: Anti-lock Braking System (ABS) and regenerative control. By accurately interpreting the signals and data received from the vehicle's sensors, the brake controller assembly is able to make real-time decisions to optimize braking performance and ensure the safety of the vehicle and its occupants. Its ability to differentiate between ABS and regenerative braking further enhances the overall functionality and reliability of the system, making it a crucial component in modern vehicle braking systems [7].

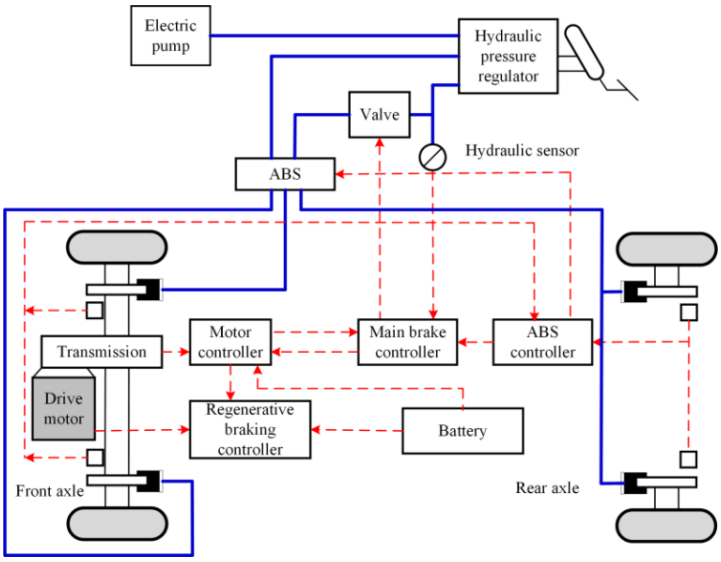

Figure1. Schematic representation of the motorized hydraulic brake system.

The regenerative braking controller, which forms the second layer, is responsible for efficiently managing the allocation of braking torque between hydraulic brakes and motor-driven forces. Its primary function is to optimize this distribution to maximize energy recovery during braking. This sophisticated system not only enhances braking performance but also contributes to improved overall vehicle efficiency by converting kinetic energy into electrical energy, which can be stored and reused. By dynamically adjusting the balance between traditional hydraulic braking and regenerative braking through the motor, the controller ensures a seamless and efficient braking experience, thereby extending the range and reducing wear on brake components.

2.2. Dynamics model of electric vehicles

For a vehicle to maintain motion, the driving force, denoted as F_t, must overcome various resistive forces that impede its progress. These resistances include rolling resistance, F_f, which emerges from the complex interplay between vehicle tires and the road surface; acceleration resistance, F_j, required to increase the vehicle's velocity; slope resistance, F_i, encountered when traveling uphill; and air resistance, F_w, caused by the friction of air against the vehicle's exterior. The driving equation for a vehicle can be represented in a general form as follows:

$$F_t = F_f + F_w + F_i + F_j. \tag{1}$$

Expanding the above forces, we get the following equations [16]:

$$\frac{T_{tq} i_g \eta_T}{r} = Gf\cos\alpha + G\sin\alpha + \frac{C_D A u_a^2}{21.15} + m\frac{\mathrm{d}u}{\mathrm{d}t}, \tag{2}$$

where, the motor's output torque is represented by T_{tq}, the transmission ratio by i_g, the vehicle's weight by G, the road gradient by i, the vehicle's speed by u_a, the vehicle's mass by $m=G/g$, and the acceleration by du/dt. The vehicle specifications include an unloaded weight of m_u=1640 kg, a full-loaded weight of m_f=1910 kg, a center of mass at h_g=0.58 m, a wheelbase of L=2.672 m, a rolling resistance coefficient of f=0.02, a driving range of S=400 km, a maximum speed of u_{max}=150 km/h, a windward area of A=2.5 m², a tire rolling radius of r=0.33 m, a mechanical efficiency of η_T=0.8, a maximum climbing slope of α_{max}=30%, and an air resistance coefficient of C_d=0.45. The distance from the front axle to the center of mass is a=1.341 m, while the distance from the rear axle to the center of mass is b=1.431 m.

The upper transmission ratio is an important factor determined by the need for the vehicle to reach its maximum speed. This relationship can be mathematically represented by the equation:

$$i_g \le 0.377 \frac{n_{max} r}{u_{max}}. \tag{3}$$

Conversely, the minimum transmission ratio is established by taking into account the motor's power output at its maximum velocity. To ensure optimal performance, the driving force should not fall below the driving resistance. This constraint can be expressed mathematically as:

$$i_g \ge n_{max} r \left(mg(f \cos\alpha_{max} + \sin\alpha_{max}) + \frac{C_d A u_i^2}{21.15} \right) \Big/ 9550 P_{me} \eta_T . \tag{4}$$

By carefully analyzing and combining the aforementioned upper and lower limit considerations, the most suitable transmission ratio for the selected gear reducer can be determined. In this particular case, after thorough calculations and evaluations, the optimal transmission ratio is found to be i_g=7. 241. This value ensures that the vehicle can achieve its maximum speed while maintaining sufficient driving force to overcome the driving resistance, thereby guaranteeing efficient and reliable performance.

2.3. Parameters of the drive motor

The following three factors can help determine the required motor power, ensuring that the vehicle's performance and driving experience meet expectations. This analysis explores the motor power requirements for a vehicle, considering three distinct scenarios:

(1) Motor power for maximum speed: The vehicle's peak velocity serves as the primary factor in determining the motor power, designated as P_1. This crucial relationship between speed capability and power output is fundamental in vehicle design and engineering. The maximum attainable speed directly influences the

required motor power, as higher velocities necessitate greater energy output to overcome increasing resistance forces. Engineers must carefully consider this correlation when developing powertrains for various vehicle types, ensuring that the motor's capabilities align with the desired performance characteristics. This relationship is mathematically represented as following:

$$P_I = \frac{u_{max}}{3600\eta_T}(mgf + \frac{C_d A u_{max}^2}{21.15}). \tag{5}$$

A higher desired maximum speed necessitates a more powerful motor to overcome the increasing aerodynamic drag and rolling resistance encountered at higher speeds.

(2) Motor power for acceleration: The motor power, denoted as P_{II}, is determined by the time it takes for the vehicle to accelerate from rest (u_e=0 km/h) to a speed of 100 km/h (u_a). This acceleration time, denoted as tm, is constrained to be less than 14 seconds. The relationship between motor power and acceleration time is represented as following:

$$P_{II} = \frac{1}{3600\eta_T}(\frac{2}{3}mgfu_a + \frac{4}{5}\frac{C_D A u_a^3}{21.15} + \frac{1}{2t_m}\mathrm{m}\frac{u_a^2 + u_e^2}{3.6}). \tag{6}$$

(3) Motor power for climbing: The motor power, denoted as P_{III}, is determined by the vehicle's ability to climb a maximum slope α_{max} at a specific speed. This speed, denoted as u_i, is specified as 35 km/h. The relationship between motor power and the maximum climbable slope is represented as following:

$$P_{III} = \frac{u_i}{3600\eta}(mgf\cos\alpha_{\max} + mg\sin\alpha_{\max} + \frac{C_D A u_i^{\,2}}{21.15}). \tag{7}$$

To satisfy the performance requirements of maximum speed, acceleration, and climbing ability, the motor's peak power must be sufficient to meet the demands imposed by each of these scenarios. P_{max} must meet or exceed the highest value found among P_I, P_{II}, and P_{III}. This requirement can be articulated as:

$$P_{max} = \max(P_I, P_{II}, P_{III}). \tag{8}$$

The motor has a rated power of P_e=37 kW at a rated speed of n_e=3600 r/min with a rated torque of T_e=97 N·m, a peak power of P_{max}=96 kW at a peak speed of n_{max}=9000 r/min with a peak torque of T_{max}=256 N·m.

2.4. Calculation of power battery State of Charge (SOC)

Meeting certain distance requirements at a steady pace is crucial to ensure that an electric vehicle has an adequate range. In particular, when the vehicle is driven at a steady speed of u_a=60 kilometers per hour, the minimum distance it should be capable of covering is S=400 km. This minimum distance requirement is crucial for matching the energy capacity of the power battery. To optimize the

performance of electric vehicles, engineers closely monitor the power battery discharge depth η_{soc}, ensuring that it remains within the optimal range for longevity and efficiency. The power battery discharge depth refers to the ratio of the amount of electricity discharged from the battery during the discharge process to its total capacity. It is usually expressed as a percentage. The greater the discharge depth, the more the battery is used, and a high discharge depth over a long period of time may affect the life of the battery. The discharge current efficiency refers to the ratio of the actual output of a battery to its theoretical output during discharge. This efficiency is affected by a number of factors, including the chemical characteristics of the battery, the temperature, the discharge rate, and so on. High efficiency means that the battery is able to utilize its stored energy more efficiently when discharged. When evaluating the overall energy management system, it's crucial to consider the discharge current efficiency η_{cut}, as it directly impacts the battery's operational effectiveness and lifespan. The calculation of energy consumption for a journey spanning a minimum of 400 kilometers while maintaining a steady velocity of 60 kilometers per hour can be determined using the following approach:

$$E_{bat} \geq \frac{mgf + C_d A u_a^{\,2} / 21.15}{3600 \times \eta_{soc} \times \eta_T \times \eta_{cut}} \times S, \tag{9}$$

where, η_{soc}=0.8 and η_{cut}=0.9 [17]. Next, we can determine the battery's capacity using the following method:

$$Q_{cap} = 1000 \frac{E_{bat}}{U_e}, \tag{10}$$

where, U_e denotes the rated voltage of the power battery.

The power battery is equipped with a rated voltage of U_e=336 V, a battery capacity of Q_{cap}=271 Ah, a maximum charging power of P_{Bmax}=111 kW, and a specific energy of E=120 Wh/kg. With the widespread adoption and development of electric vehicles, State of Charge (SOC) monitoring and estimation have become a focal point of research in electric vehicle technology. The driving range of electric vehicles is directly correlated with the accuracy of SOC estimation, and researching and developing precise and reliable SOC estimation methods is crucial for enhancing vehicle performance and user experience. the current integration method is currently one of the most prevalent SOC estimation approaches in battery management systems, fundamentally involving the estimation of battery SOC by accumulating the charge entering or discharged from the battery during charging or discharging processes. Estimating the battery's state of charge (SOC) can be achieved through the current integration method [18].

$$SOC = SOC_{ini} - \frac{1}{3600 Q_{cap}} \int \eta_b I_m dt, \tag{11}$$

The initial battery state of charge (SOC_{ini}) is represented by SOC_{ini}=0.95. The current (I_m) is a crucial factor in the charging and discharging operations. This

approach involves the real-time measurement of the primary circuit current of the battery pack. Notably, a negative current signifies the charging process, while a positive current signifies the discharging process.

It becomes possible to derive an equation for calculating the driving current that drives the vehicle, denoted as I_m, flowing through the main circuit of the vehicle's electrical system, expressed as follows:

$$I_m = \frac{\eta_b T_{tq} n}{9.55 U_{ec}}. \tag{12}$$

Regenerative braking operates by reversing the motor's role when the vehicle decelerates. Instead of consuming electrical energy to create motion, the motor generates electricity by capturing the kinetic energy that would otherwise be lost as heat during conventional braking. This converted energy is subsequently stored in the vehicle's battery for future use. The mathematical representation of the generated current, denoted as I_m, can be expressed through the following equation:

$$I_m = \frac{-\eta_b T_{tm} n}{9.55 U_{ec}}, \tag{13}$$

where, the braking torque of the motor, denoted by T_{tm}, is a critical parameter that determines the motor's ability to slow down or come to a complete stop. This torque is influenced by the motor's rotational speed, represented by n, and the voltage at the power battery terminal, designated as U_{ec}. To better understand the relationship between these variables, it is essential to examine the formula for U_{ec}, which is given by $U_{ec}=U_e–I_mR$. This equation highlights the dependence of U_{ec} on the internal resistance of the battery, R, which typically ranges from 0.015 to 0.06.

2.5. Quantifying Recovered Energy

Regenerative braking is a method used to recover and store energy in the battery. The recovered energy, represented as E_r, can be determined by employing the following mathematical equation:

$$E_r = \int_{braking} U_{oc} I_m dt. \tag{14}$$

The total energy consumption of the vehicle, denoted as E_{tol}, can be determined by considering various factors such as the vehicle's weight, aerodynamic drag, rolling resistance, and powertrain efficiency. This energy requirement is influenced by the vehicle's speed, driving conditions, and the distance traveled. The total energy consumption can be quantified as follows:

$$E_{total} = \int_{driving} U_{oc} I_m dt. \tag{15}$$

In an electric vehicle that does not have regenerative braking capabilities, the vehicle is unable to convert the kinetic energy generated during braking back into electrical energy to recharge the battery. The difference in state of charge (SOC_n)

from the starting state of charge (SOC_{int}) to the ending state of charge (SOC_{end}) is directly related to the E_{tot} while braking. When an electric vehicle is in operation, its state of charge (SOC) undergoes fluctuations. However, when regenerative braking is employed, the SOC change (SOC_y) incorporates not only the total energy consumption (E_{tot}) but also the recovered energy (E_r). As a result, the SOC_y is influenced by the interplay between the energy consumption and recovery processes. The formula for calculating the regenerative braking recovery efficiency (ε) is:

$$\varepsilon = \frac{E_r}{E_{tot}} = \frac{\Delta SOC_n - \Delta SOC_y}{\Delta SOC_n}. \tag{16}$$

2.6. Two driving cycles

Standardized test procedures known as driving cycles are utilized to assess the fuel consumption and emissions of vehicles. The electric car driving cycle test assesses how well electric vehicles perform and consume energy in actual driving conditions. The process replicates the performance of the car in various driving scenarios like speeding up, slowing down, and maintaining a consistent pace, to provide a more precise evaluation of the electric vehicles' range and energy usage.

WLTC and CLTC-P are two standardized driving test cycles that assess the fuel efficiency and emissions of vehicles, as depicted in Fig. 2. WLTC is a more recently developed driving cycle that aims to better represent real-world driving conditions. It includes a wider range of driving speeds, accelerations, and road types, making it more representative of actual vehicle usage. In China, CLTC-P is the standard driving cycle for evaluating the fuel efficiency and emissions of vehicles. It is designed to reflect the unique driving conditions and traffic patterns in China, with a focus on urban and suburban driving.

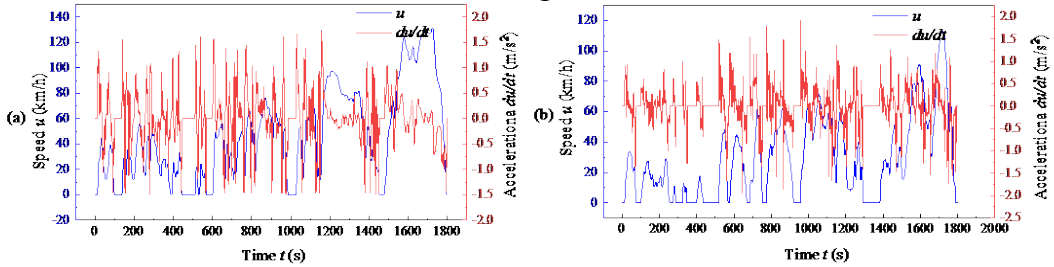

Figure 2. Two curves representing the speed u and acceleration du/dt: (a) WLTC and (b) CLTC-P.

3. Braking force distribution

3.1. Distribution of braking force between the front and rear axles

The distribution of braking force has a profound effect on the overall braking performance, as varying conditions can significantly influence the vehicle's behavior. Inadequate distribution can lead to compromised stability, reduced traction, and increased stopping distances, whereas an optimal distribution can enhance the vehicle's responsiveness, improve cornering capabilities, and reduce the risk of wheel lock-up or skidding. We suggests a braking force distribution strategy that changes the allocation of braking force between the front and rear wheels in multiple stages. This strategy is developed by harmonizing two key elements:

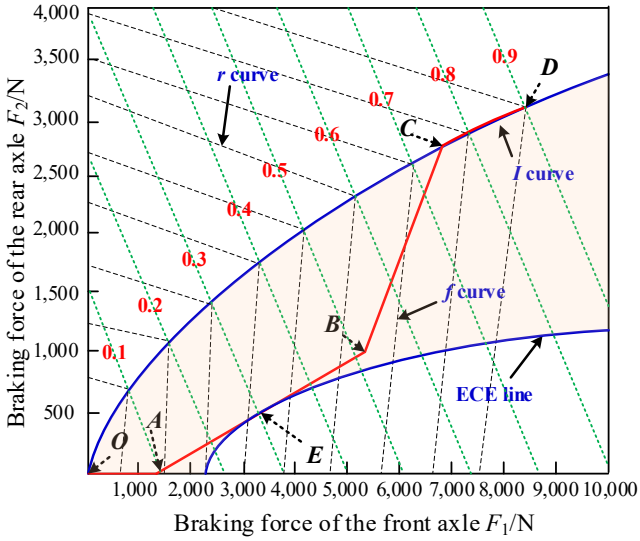

Figure 3. Strategies for distributing braking forces between front and rear wheels [18].

(1) The ideal braking force distribution (*I*-curve) [19]: In the design of automotive braking systems, the purpose of ensuring that the front and rear brakes can lock simultaneously under different road adhesion conditions is to improve the stability of vehicle braking and the rationality of braking force distribution. At this point, the relationship curve between the braking forces $F_{\mu 1}$ and $F_{\mu 2}$ of the brakes is called the *I*-curve. The ideal braking force distribution curve is determined by comprehensively considering factors such as the vehicle's center of gravity position, center of gravity height, axle load distribution, and longitudinal dynamic load transfer during the actual braking process. This curve can effectively ensure the vehicle always maintains optimal stability and safety during the braking process.

(2) ECE regulations [20]: ECE regulations are a series of standards regarding automotive and motorcycle safety issued by the Economic Commission for Europe, having become a significant regulation in the automotive and motorcycle industries in the European region. Within the ECE regulations, the requirements for the brake force distribution curve are specified in three types: Type I curve: In the case of simultaneous locking and skidding of both front and rear

wheels, the brake force distribution curve for the front and rear axles should be of Type I. Type II curve: In the event that either the front wheels or the rear wheels lock and skid, the brake force distribution curve for the front and rear axles should be of Type II. Type III curve: In other situations, the brake force distribution curve for the front and rear axles should be of Type III.

In Fig. 3, the braking forces applied by the front and rear axles are denoted as F_1 and F_2, respectively, with the coordinate origin labeled as point *O*. At point *A*, the transverse coordinate corresponds to a braking force *z* of 0.1, signifying low-intensity braking. Moving along section *AB*, the braking intensity increases to a medium level. High-intensity braking is then implemented in section *BC*, leading to emergency braking in section *CD*. To enhance braking performance and safety, only hydraulic braking is authorized during the emergency braking phase denoted by section *CD*.

(1) If the braking power z is 0.1 or lower, the vehicle will have weak braking power and will heavily depend on the front wheels for braking force. In this operating condition, the front axle takes on the primary responsibility of slowing down the vehicle. The braking force distribution rule can be mathematically represented as:

$$\begin{cases} F_1 = Gz \\ F_2 = Gz - F_1 \end{cases}. \tag{17}$$

(2) If the braking intensity is between 0.1 and 0.505, which is for section *AB*, the ECE regulation requires the braking distribution to be higher than the specified ECE curve. The simultaneous engagement of both axles in the braking process is an essential requirement to ensure optimal vehicle stability and control during deceleration within this particular braking strength range, represented as:

$$\begin{cases} F_1 = \dfrac{Gz + 0.02268G}{1.2268} \\ F_2 = Gz - F_1 \end{cases}. \tag{18}$$

(3) When the braking strength is between 0.505 and 0.665, the principle for distributing braking force is as follows:

$$\begin{cases} F_1 = 0.95\varphi h_g \dfrac{Gz + Gb/h_g}{L} \\ F_2 = Gz - F_1 \end{cases}, \tag{19}$$

where φ represents the coefficient of road adhesion.

(4) Emergency braking is initiated when the braking strength exceeds a threshold value of z=0. 665. In this scenario, particularly the *CD* section, the regulation for distributing braking force is as follows:

$$\begin{cases} F_1 = G\varphi \dfrac{b + zh_g}{L} \\ F_2 = G\varphi \dfrac{a - zh_g}{L} \end{cases}. \tag{20}$$

3.2. Distribution of braking force on the front axle

As demonstrated in Fig. 4, when actively driving a vehicle, it becomes imperative to take into account a multitude of factors in order to effectively harness regenerative braking and optimize energy efficiency. The integration of regenerative braking with a hydraulic braking system necessitates a strategic allocation of braking force to capitalize on energy recuperation opportunities.

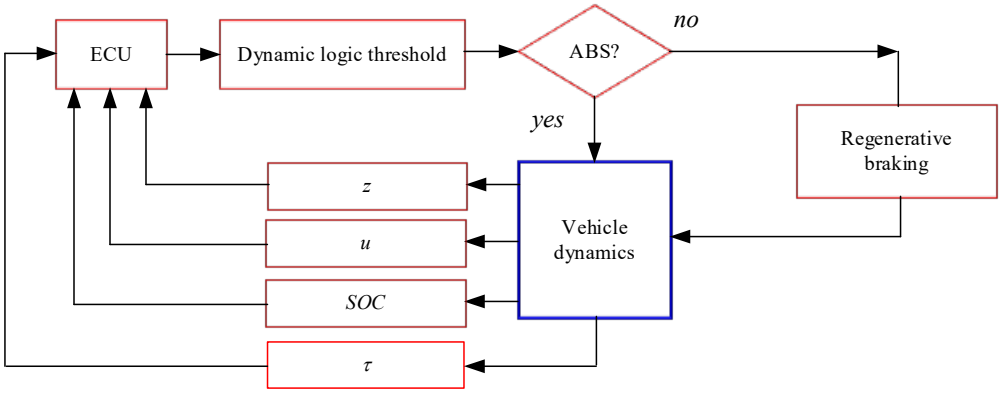

Figure 4. Algorithm for controlling regenerative braking with dynamic logic threshold.

(1) Regenerative braking force, a crucial element in modern braking systems, is determined by a limiting distribution coefficient that is directly impacted by the braking intensity, represented as k_z. This coefficient, which serves as a key performance indicator, can be mathematically expressed as follows:

$$k_z = \begin{cases} 1, \ z \le a_1, \\ -\dfrac{500}{405} z + \dfrac{455}{405}, \ a_1 < z \le b_1, \\ 3.125(0.665 - z), b_1 < z \le c_1, \\ 0, \ z > c_1, \end{cases}, \tag{21}$$

where, a_1=0.1, b_1=0.505, and c_1=0.665.

(2) The distribution of regenerative braking force is governed by a speed-dependent coefficient, which can be mathematically expressed as a function of the vehicle's velocity u_a (km/h). This coefficient plays a crucial role in optimizing the energy recovery process during deceleration and braking events. This relationship can be expressed mathematically as follows [18]:

$$k_u = \begin{cases} 0, \ u \le a_2, \\ -0.5(8-u), \ a_2 < u \le b_2, \\ 1, \ b_2 < u \le c_2, \\ -(u-200)/80, \ c_2 < u \le d_2, \\ 0, \ u > d_2, \end{cases}, \tag{22}$$

where, a_2=8, b_2=15, c_2=120, d_2=200.

(3) The distribution coefficient that limits regenerative braking force, which is determined by state of charge (*SOC*), can be represented as follows:

$$k_{SOC} = \begin{cases} 0, \ SOC > a_3, \\ 20(0.95 - SOC), \ a_3 < SOC < b_3, , \\ 1, \ SOC \le b_3, \end{cases} \tag{23}$$

where, a_3=0.95, b_3=0.9.

(4) Frequent charge and discharge cycles may lead to a reduction in the lifespan of power batteries. Avoiding regenerative braking within closely adjacent braking intervals can minimize the battery's charge-discharge frequency, thereby reducing the risk of battery thermal degradation and extending its service life. However, if the subsequent braking intensity is significantly high (i.e., z>0.2), regenerative braking should be engaged despite its potential impact on the battery, as the energy recovery rate during braking would be substantially high. The braking interval factor is represented as follows: :

$$k_\tau = \begin{cases} 1, \mathrm{sgn}(z-0.3) > 0, \\ \mathrm{sgn}(t_b - 2), \mathrm{sgn}(z-0.3) \le 0, \end{cases}, \tag{24}$$

where sgn represents the sign function, and t_b (s) denotes the time interval between two adjacent braking events.

Consequently, the total distribution coefficient for the participation ratio of regenerative braking at the front axle can be represented as follows:

$$k = k_z \cdot k_u \cdot k_{SOC} \cdot k_\tau. \tag{25}$$

By utilizing the overall distribution coefficient k, the system can automatically modify the threshold for the percentage of regenerative braking involvement at the front axle, ultimately enhancing the system's performance and stability.

The peak regenerative braking torque of an electric motor is influenced not only by its inherent electrical properties but also by the constraints of the battery's electrical characteristics. For example, one constraint is the motor's ability to convert kinetic energy back into electrical energy efficiently. Another limitation is the battery's capacity to accept the regenerated energy at a high rate without overheating or degrading. Additionally, the overall system must manage the energy

flow to prevent over-voltage conditions, which can affect performance and safety. Therefore, the interplay between the motor's efficiency and the battery's acceptance rate predominantly determines the upper limit of regenerative braking torque. Several key factors limit the maximum regenerative braking torque [21]:

(1) Generated power: The amount of electrical energy generated through regenerative braking is limited by the motor's power output.

(2) Motor speed: Higher speeds result in greater energy generation, but below a certain minimum speed, the energy recovery becomes negligible.

(3) Battery charging capacity: The battery pack has an upper limit on the charging current it can accept, restricting the energy recovery.

The formula for determining the highest braking force of the electric motor T_{emax} can be calculated using the following form [18]:

$$T_{emax}=\begin{cases}\min\left[\dfrac{9550P_{max}}{n} \quad \dfrac{9550P_{Bmax}}{\eta_{cut}n}\right], & n>n_e\\ \min\left[T_{max} \quad \dfrac{9550P_{Bmax}}{\eta_{cut}n_e}\right], & n_{min}\le n\le n_e,\\ 0, & n\le n_{min}\end{cases} \tag{26}$$

where, the motor's maximum power is referred to as P_{max}, the battery's highest charging power is denoted as P_{Bmax}, the charging efficiency of the battery is represented as η_{cut}, and the motor's maximum torque is indicated by T_{max}. Furthermore, the motor's minimum speed is n_{min}, which is 356 $r\cdot\min^{-1}$.

A judicious balance between hydraulic (F_{hyd}) and regenerative (F_{reg}) braking forces within the system is crucial to guarantee the provision of adequate braking force for the vehicle. This equilibrium is typically maintained through the equation $F_1=F_{hyd}+F_{reg}$. In cooperative braking mode, the primary goal is to maximize energy recovery while ensuring safe and efficient deceleration. This strategic distribution of braking forces enables optimal energy recovery. The correlation between hydraulic brake force and regenerative brake force can be represented as follows [18]:

$$\begin{cases}\begin{cases}F_{reg}=T_{emax}i_g i_0/r\\ F_{hdy}=F_1-F_{reg}\end{cases}, & if\ \ kF_1 r/\left(i_g i_0\right)\ge T_{emax}\\ \begin{cases}F_{reg}=F_1 k\\ F_{hdy}=F_1-F_{reg}\end{cases}, & if\ \ kF_1 r/\left(i_g i_0\right)<T_{emax}\end{cases}, \tag{27}$$

4. Simulation and analysis

Matlab/Simulink provides a comprehensive environment for creating detailed simulations that incorporate various dynamic variables and control logic

thresholds. Such simulations enable the identification of optimal control parameters that can enhance the efficiency and safety of the braking system.

4.1. Variations of braking forces

Fig. 5 demonstrates that the observed braking strength predominantly falls below the 0.15 mark. To maximize the regenerative braking force, the majority of the torque is allocated to the front axle. This strategic distribution of braking force not only enhances energy recovery efficiency but also significantly improves the overall driving experience. By optimizing how the braking force is spread across the vehicle's axles, the system can make full use of the regenerative braking capabilities inherent in electric vehicles.

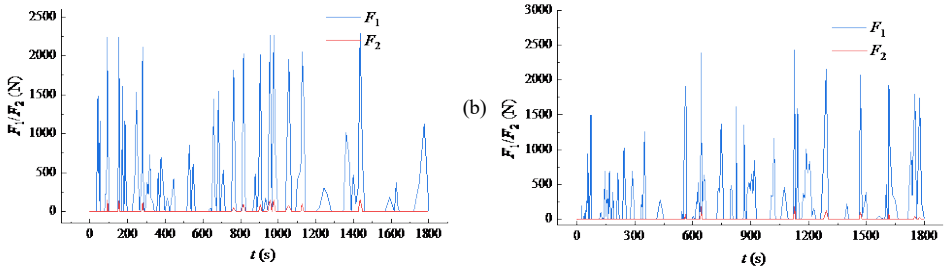

Figure 5. Comparison of braking forces distributed between front and rear axles under different driving cycles: (a) WLTC and (b) CLTC-P.

As shown in Fig. 6, under moderate braking conditions, the regenerative braking system effectively recovers a considerable amount of kinetic energy. This system is capable of contributing a significant proportion to the total braking force, thereby improving the efficiency of energy recovery. This implies that during typical driving scenarios, the regenerative braking system is highly effective in converting kinetic energy into electrical energy, which can then be stored in the vehicle's battery for future use. By managing the distribution of braking forces more effectively, electric vehicles not only improve their range through better energy recovery but also deliver a smoother and more controlled braking experience.

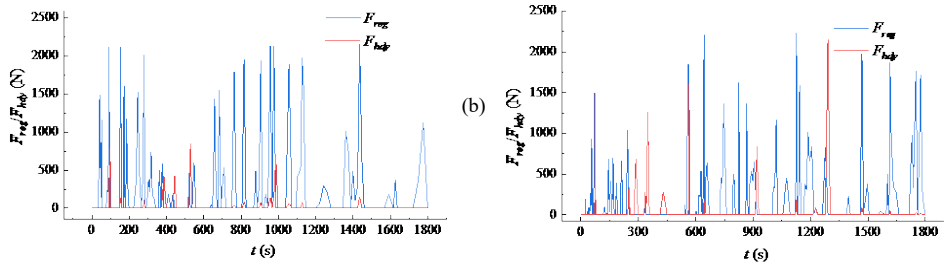

Figure 6. Front axle braking force distribution: Comparison of hydraulic and motor contributions under (a) WLTC and (b) CLTC-P cycles.

4.2. Fluctuations in distribution coefficient k

Fig. 7 illustrates the fluctuation of the distribution coefficient across two distinct driving scenarios. The average distribution coefficients for the two driving cycles are recorded as 0.38 and 0.33, respectively. This data reveals a notable trend: the WLTC driving cycle exhibits a significantly higher proportion of motors engaged in regenerative braking compared to the CLTC-P cycle. This disparity in motor utilization underscores the distinct characteristics of these driving conditions and their impact on the distribution of energy flow within the system.

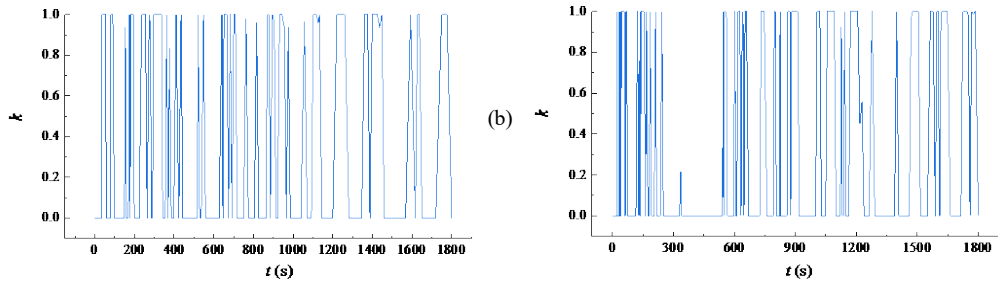

Figure 7. Variations of distribution coefficient k: (a) WLTC and (b) CLTC-P.

4.3. Variations of current I_m

Fig. 8 illustrates the current performance of the engine throughout one complete driving cycle. This figure provides valuable insights into the motor's current demands under various driving cycles.

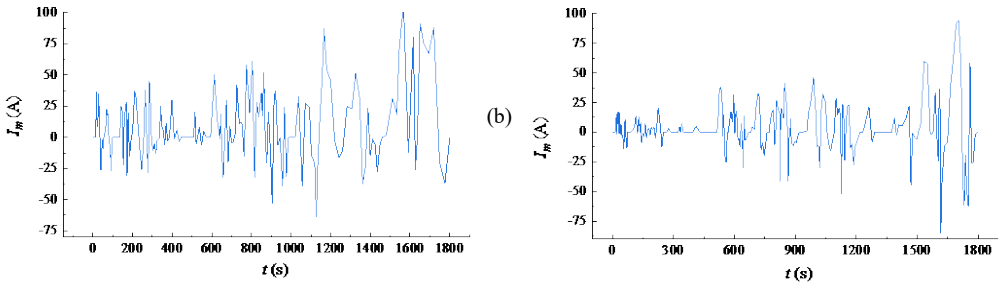

Figure 8. Variations of current Im: (a) WLTC and (d) CLTC-P.

The maximum discharge currents for the two driving cycles are measured as 106.96 A and 94.17 A. The maximum charging currents are recorded as –63.56 A and –85.31 A. The negative sign indicates that the motor is operating in regenerative braking mode, where it converts kinetic energy back into electrical energy, effectively charging the battery. Furthermore, we calculate the average discharge and charging currents for each driving cycle. The average discharge currents are found to be 15.66 A and 9.27 A.The average charging currents are –6.61 A and –4.54 A, suggesting the average amount of current returned to the battery during regenerative braking. The data provides insights into the battery's performance and the effectiveness of the regenerative braking system during the two driving cycles.

4.4. SOC variations

As shown in Fig. 9, simulation starts with an initial SOC_{int}=0.9, which gradually declines as the driving cycle progresses. This contrasts with the monotonic decrease observed in vehicles without regenerative braking. As the vehicle travels and brakes, the *SOC* curves diverge, with regenerative braking leading to a more fluctuating *SOC* variation.

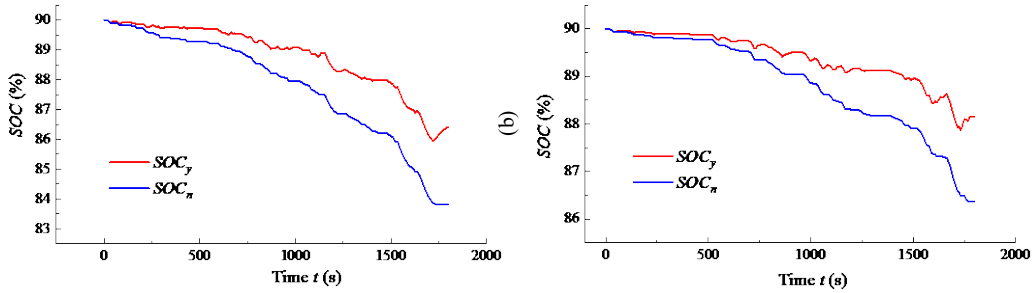

Figure 9. SOC variations: (a) WLTC and (d) CLTC-P.

Table 1 reveals that the SOC_y values under the WLTC and CLTC-P cycles are 86.47% and 88.23%, respectively. Simultaneously, the corresponding SOC_n values are 83.82% and 86.51%, respectively. Consequently, the calculated energy recovery efficiency for these cycles are ε=43.58% and 49.86%, respectively.

Table 1.

SOC analysis and comparison.

Driving cycle	Without regenerative braking			with regenerative braking			ε/%
	SOC_{int}/%	SOC_n/%	ΔSOC_n/%	SOC_{int}/%	SOC_y/%	ΔSOC_y/%	
WLTC	90	83.82	6.18	90	86.51	3.49	43.58
CLTC-P	90	86.47	3.53	90	88.23	1.77	49.86

4.5. Energy recovery performance

As shown in Fig. 10, both E_{tol} and E_{reg} exhibit an upward trajectory, with E_{tol} consistently surpassing E_{reg} by a considerable margin. Specifically, under the WLTC, the data reveals a total energy consumption E_{tol} of 2450. 25 kJ and a total energy recovery E_{reg} of 1054. 97 kJ. Conversely, in the CLTC-P, the total energy consumption E_{tol} is notably lower at 1464.81 kJ, with energy recovery E_{reg} amounting to 722.31 kJ. This comparative analysis underscores the variations in energy dynamics dependent on the driving conditions, reflecting differing demands on the vehicle's energy systems. The higher E_{tol} values compared to E_{reg} indicate that electric vehicles still consume more energy than they are able to recover, even with the implementation of energy recovery systems. The regenerative braking efficiency consistently exceeded 40% for two consecutive driving cycles.

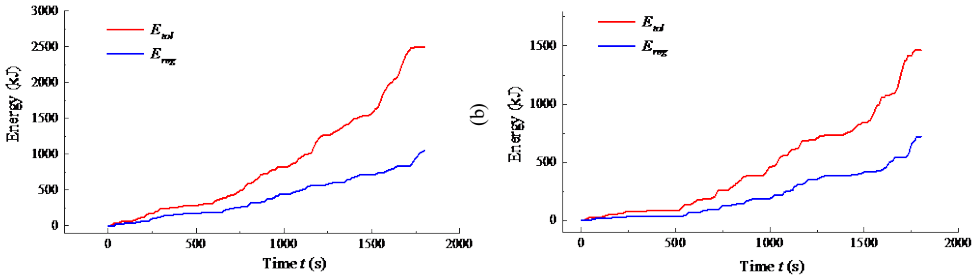

Figure 10. Variations of Etol and Ereg: (a) WLTC and (b) CLTC-P.

5. Conclusion

This study presents a dynamic logic threshold control strategy for regenerative braking in electric vehicles. The goal of this strategy is to maximize energy recovery while maintaining vehicle stability and adhering to braking regulations. The results present a dynamic logic threshold strategy for regenerative braking, significantly enhancing energy recovery efficiency. Vehicles with regenerative braking show an increase in energy recovery efficiency of 43.58% and 49.86% under two different cycle conditions compared to those without regenerative braking. The research highlights the significance of a dynamic logic threshold control strategy for enhancing energy recovery efficiency in electric vehicles through regenerative braking. However, areas for improvement include further optimization of the strategy to ensure consistent vehicle stability and compliance with braking regulations. Future developments could focus on integrating advanced control algorithms and sensor technologies to enhance the performance and applicability of regenerative braking systems in a wider range of driving scenarios.

Acknowledgements

Funding for this study was provided by the University Natural Science Research Project of Anhui Province under grant numbers KJ2021A1205 and 23kytdpy001, and the Intelligent Detection Research Team Funds for the Anhui Institute of Information Technology under grant numbers AXG2023_kjc_5004, 2021xnfzxm047, 2023sx153 and 23QNJJKJ015.

REFERENCES

[1] C. *Fiori, K. Ahn, and H. Rakha*, "Power-based electric vehicle energy consumption model: Model development and validation", *Appl. Energ.*, vol. 168, pp. 257-268, Apr. 2016. (Article)

[2] *A. Hamada, and M. Orhan*, "An overview of regenerative braking systems", *J. Energy Storage*, vol. 52, pp. 105033, Aug. 2022. (Article)

[3] *P. Saiteja, B. Ashok, A. Wagh, and M. Farrag*, "Critical review on optimal regenerative braking control system architecture, calibration parameters and development challenges for EVs", Int. J. Energ. Res., vol. 46, pp. 20146-20179, Nov. 2022.

[4] *H. Jamil, S. Naqvi, N, Iqbal, M, Khan, F. Qayyum, F. Muhammad, S. Khan, and D. Kim*, "Analysis on the Driving and Braking Control Logic Algorithm for Mobility Energy Efficiency in Electric Vehicle", Smart Grid. Sust. En., vol. 9, pp. 12, Feb. 2024.

[5] *J. Ko, S. Ko, H. Son, B. Yoo, J. Cheon, and H. Kim*, "Development of Brake System and Regenerative Braking Cooperative Control Algorithm for Automatic-Transmission-Based Hybrid Electric Vehicles", *IEEE T. Veh. Technol.*, vol. 64, pp. 431-440, Feb. 2015.

[6] *G. Xu, W. Li, K. Xu, and Z, Song*, "An Intelligent Regenerative Braking Strategy for Electric Vehicles", Energies, vol. 4, pp. 1461-1477, Sep. 2011

[7] *Z. Yin, X. Ma, R. Su, Z. Huang, and C. Zhang*, "Regenerative Braking of Electric Vehicles Based on Fuzzy Control Strategy", Processes, vol. 11, pp. 2985, Oct. 2023.

[8] *S. Heydari, P. Fajri, M. Rasheduzzaman, and R. Sabzehgar*, "Maximizing Regenerative Braking Energy Recovery of Electric Vehicles Through Dynamic Low-Speed Cutoff Point Detection", *IEEE T. Transp. Electr.*, vol. 5, pp. 262-270, Mar. 2019

[9] *C. Yang, T. Sun., W. Wang, Y. Li, Y. Zhang, and M. Zha*, "Regenerative braking system development and perspectives for electric vehicles: An overview", Renew. Sust. Energ. Rev., vol. 198, pp. 14389, Jul. 2024.

[10] *Y. Zhang, W, Wang, C. Xiang, C. Yang, H. Peng, and C. Wei*, "A swarm intelligence-based predictive regenerative braking control strategy for hybrid electric vehicle", Vehicle Syst. Dyn., vol. 60, pp. 973-997, Mar. 2022.

[11] *C. Qiu, and G. Wang*, "New evaluation methodology of regenerative braking contribution to energy efficiency improvement of electric vehicles", Energ. Convers. Manage., vol. 119, pp. 389-398, Jul. 2016.

[12] *Maia. R, Silva. M, Araújo. R and Nunes. U,* "Electrical vehicle modeling: A fuzzy logic model for regenerative braking", in Expert Systems with Applications, vol. 42, Dec. 2015, pp. 8504-8519

[13] J. *Hao, Z. Yu, Z. Zhao, P. Shen, and X. Zhan*, "Optimization of Key Parameters of Energy Management Strategy for Hybrid Electric Vehicle Using DIRECT Algorithm", Energie*s*, vol. 9, pp. 997, Dec. 2016.

[14] *G. Sandrini, D. Chindamo, and M. Gadola*, "Regenerative Braking Logic That Maximizes Energy Recovery Ensuring the Vehicle Stability", Energies, vol. 15, pp. 5846, Aug. 2022.

[15] *J. Hu, X. Lin, D. Yin, and F. Hu*, "Dynamic motion stabilization for front-wheel drive in-wheel motor electric vehicles", Adv. Mech. Eng., vol. 7, pp. 1687814015623694, Dec. 2015.

[16] *X. Wang, S. Shi, L. Liu, and L. Jin*, "Analysis of driving mode effect on vehicle stability", *Int.* J. Auto. Tech-Kor, vol. 14, pp. 363-373, Jun. 2013. (Article)

[17] *O. Demirci, S. Taskin, E. Schaltz, B. Demirci*, "Review of battery state estimation methods for electric vehicles - Part I: SOC estimation", J. Energy Storage, vol. 87, pp. 111435, May. 2024.

[18] *Z. Yin, X. Ma, C. Zhang, R. Su, and Q. Wang*, "A Logic Threshold Control Strategy to Improve the Regenerative Braking Energy Recovery of Electric Vehicles", Sustainability-Basel, vol. 15, pp. 16850 Dec. 2023.

[19] *S. Li, B. Yu, and X. Feng,* "Research on braking energy recovery strategy of electric vehicle based on ECE regulation and *I* curve", Sci. Progress-UK, vol. 103, pp. 0036850419877762, Jan. 2020.

[20] *T. Liu, J. Zheng, Y. Su, and J. Zhao*, "A Study on Control Strategy of Regenerative Braking in the Hydraulic Hybrid Vehicle Based on ECE Regulations", Math. Probl. Eng., vol. 103, pp. 208753, Dec. 2013.

[21] *Y. Park, S. Park, and C. Ahn*, "Performance Potential of Regenerative Braking Energy Recovery of Autonomous Electric Vehicles", Int. J. Control Autom., vol. 21, pp. 1442-1454, May. 2023.